Regular Article

Electro-optical properties of solution-processed aluminum–nickel oxide film containing graphene oxide in liquid crystal system

Jin Young Oh[1]**, Eun Mi Kim**[2]**, Gi Seok Heo**[2]**, Da Bin Yang**[1]**, Bo-Kyeong Choi**[1]**, Dong Hyun Kim**[3]**, Dong Wook Lee**[4,a]**, Dae-Shik Seo**[1,b] (ID)

[1] IT Nano Electronic Device Laboratory, Department of Electrical and Electronic Engineering, Yonsei University, Seodaemun-gu, Seoul 120-749, Republic of Korea
[2] National Center for Nanoprocess and Equipment, Korea Institute of Industrial Technology, 6 Cheomdangwagi-ro 208beon-gil, Buk-gu, Gwangju 500-480, Republic of Korea
[3] Department of Electronic Engineering, Cheongju University, 298 Daesung-ro, Cheongju 28503, Republic of Korea
[4] Department of Electrical and Electronic Engineering, Jeonju University, 303 Cheonjam-ro, Wansan-gu, Jeonju-si, Jeollabuk-do 55069, Republic of Korea

Abstract Aluminum–nickel oxide and graphene oxide hybrid films are investigated in this study. The films produced via solution processing were doped with GO at three concentrations: 0, 5, and 15 wt%. The optical transmittances of the produced hybrid AlNiO films were examined for liquid crystal device applications, and their chemical properties were assessed via X-ray photoelectron spectroscopy. Atomic force microscopy and line profiling were used to examine the film surfaces. Polarized optical microscopy and pretilt angle analysis were used to confirm the uniform and homogeneous LC alignment on the hybrid AlNiO layer. The anisotropic oriented nano/microgroove structures on the surfaces of the films are believed to be due to the shear stress generated by the brush-coating process. LC cells assembled using the hybrid films showed stabler and faster switching performances with increasing GO doping. GO doping of the pure AlNiO film was also noted to increase the LC polar anchoring energy.

1 Introduction

Modification and control of the surface morphology during thin-film processing is an important research challenge in modern engineering. In particular, surfaces with nano/microgroove structures can significantly improve the performances of functional devices in optical, mechanical, and electrical applications over flat surfaces [1–3]. In electro-optics, the device properties can be controlled by introducing surface anisotropy and adjusting the surface energies through surface modifications. Nano/microstructures with undulating characteristics can also enhance the optical properties of solar cells and aid optical applications, such as liquid crystal (LC) devices [4–7].

The conventionally used film-treatment process for LC devices is the rubbing process, where a polyimide (PI) material is used as the alignment layer produced with a high-speed rotating fabric roller. The intense mechanical contact between the roller and film produces a microgroove structure, and this anisotropic structure induces uniform LC alignment on the layer. These uniformly aligned LCs can guide light unidirectionally via their permittivity and refractive index anisotropy, thereby controlling light as intended in the electronic device [8, 9]. However, the rubbing method has limitations, such as crack, defect, and electrostatic generation [10].

The solution-coating process is useful for controlling film properties, such as orientation and crystallization, making it a suitable film manufacturing process for functional device applications. It is also suitable for overcoming the limitations of the rubbing process that involves intense mechanical contact. Solution coating has excellent advantages, such as nonvacuum processing, economic efficiency, and large-scale processing capability. The brush-coating method based on the solution process can be used to deposit films with directionality; it can also simplify the fabrication process of the LC alignment layer (film deposition with subsequent alignment layer treatment) into a single step that is cost-effective while providing high throughput. Therefore, we used the brush-coating method for film construction in this study.

Aluminum–nickel oxide (AlNiO) is used as the base alignment layer in this work. Nickel oxide has good dielectric properties, which indicates its electro-optical (EO) potential for LC devices [11]. Aluminum oxide is a high-k material that also has good electrical characteristics, making it suitable for use as a dielectric [12, 13]. We doped graphene oxide (GO) in AlNiO because of the versatile properties of GO, namely electrical conductivity, mechanical stability, and film production applicability [14]; GO can also

---

[a] e-mail: dongwlee@jj.ac.kr (corresponding author)

[b] e-mail: dsseo@yonsei.ac.kr (corresponding author)

be easily utilized in solution processing because of its high solubility in water [15, 16]. The doping concentration is set to 0, 5, and 15 wt%.

X-ray photoelectron spectroscopy (XPS) was used to confirm the production of the GO-doped AlNiO hybrid films. Then, atomic force microscopy (AFM) and corresponding line profiling analysis were used to identify the anisotropic surface of each produced hybrid film having nano/microgroove structures. Next, ultraviolet–visible-near-infrared (UV–Vis-NIR) spectroscopy observations were used to assess the fine optical transmittances of the films. Polarized optical microscopy (POM) and LC pretilt angle analyses were performed to confirm the uniform and homogeneous LC alignment states on the hybrid film surfaces. The EO performances of the films were further demonstrated in a twisted-nematic (TN) LC system, and the electrical property of the film, namely the polar anchoring energy, was verified in an antiparallel LC system.

2 Experiments

2.1 Graphene and aluminum–nickel oxide hybrid film production

A 0.1 M solution of AlNiO was prepared using nickel (II) chloride hydrate and aluminum nitrate nonahydrate (ACS reagent, $\geq 98.0\%$) in equal ratios, and 2-methoxyethanol solution purchased from Sigma-Aldrich was used. A graphene oxide solution (2 mg/mL dispersion in H_2O) was used to produce the hybrid solutions. The two solutions were then blended so as to obtain AlNiO with 0, 5, and 15% GO doping. The blending was performed under 360 rpm and 75 °C condition for 2 h. The 1 d aged solution was used to wet the brush hairs thoroughly. Plain glass samples of size 2×3 cm were used for the substrates. Before coating, the substrates were thoroughly cleaned using isopropyl alcohol and acetone via ultrasonication and dried in N_2 gas. The wet brush hairs were then swept over the prepared substrates unidirectionally, followed by thermal curing at 260 °C for 1 h to obtain the GO-doped hybrid AlNiO films.

2.2 Properties of the produced hybrid films

UV–Vis-NIR spectroscopy (JASCO Corporation, V-650) was used to examine the optical transparency of each hybrid film. To ensure reliability, each sample was measured three times, and the average value was derived to create the graph. The chemical characteristics of the hybrid films were examined by XPS measurements (K-alpha, Thermo Scientific). A monochromatic Al X-ray source of 12 kV/3 mA power (Al Ka line: 1486.6 eV) was used for the measurements. The physical film surface structures were examined by AFM, and subsequent line profiling was performed to analyze the morphological properties (NX-10, Park Systems).

### 2.3 Hybrid film application to LC alignment layer

Antiparallel LC cells with a uniform cell gap of 60 μm were produced using the various GO-doped hybrid films to examine the LC alignment states. The positive-nematic LCs with $\Delta n = 0.111$, ne = 1.595, and no = 1.484 properties were used (IAN-5000XX T14; JNC); the cells were filled with LCs using a syringe via capillary force. POM (BXP 51, Olympus) measurements and pretilt angle investigations based on the oscillated transmittance values were then performed (Autronic TBA 107). Then, TN-LC cells with a 5-μm cell gap were produced to assess the EO properties. An LCD evaluation system (LCMS-200, Sesim) was used to measure the response times and voltage–transmittance curves. The LC polar anchoring energy of each cell was examined by measuring the corresponding capacitance − voltage curve using an LCR meter (Agilent 4284A).

3 Results and discussion

The optical transmittance graphs of the brush-coated GO-doped hybrid AlNiO films are shown in Fig. 1. The stable and high optical transmittance of the film is an important factor for LC device applications. The transmittance curves were obtained in the wavelength range of 250–850 nm. The visible region (380–740 nm) is indicated by the light-blue arrow in the graph. In this region, the measured transmittances show stable curves without large fluctuations, indicating the optical stabilities of the hybrid AlNiO films. The average transmittances in this region were 88.4%, 80.1%, and 80.0% for the 0, 5, and 15 wt% GO-doped AlNiO films, respectively. Considering that the average transmittances of plain and indium-tin-oxide-coated glasses are 85.4% and 81.8% in this region, the aforementioned results indicate the feasibility of the hybrid AlNiO films for LC device applications [17].

The LC alignment states of the cells based on the brush-coated GO-doped hybrid AlNiO films were evaluated by POM, as shown in Fig. 2. The LC cells were placed between the polarizer and analyzer; light from the bottom passed through the polarizer, LC cell, and analyzer in order before exiting for observation. Uniformly aligned LCs in the cell can guide the polarized light unidirectionally, and this light can be blocked when the polarizer and analyzer are vertically crossed. On the other hand, the polarized light is transmitted when the polarizer and analyzer are parallelly configured. The observed POM results show that the fabricated LC cells

Fig. 1 Transmittance curves of the AlNiO films doped with 0, 5, and 15 wt% graphene oxide
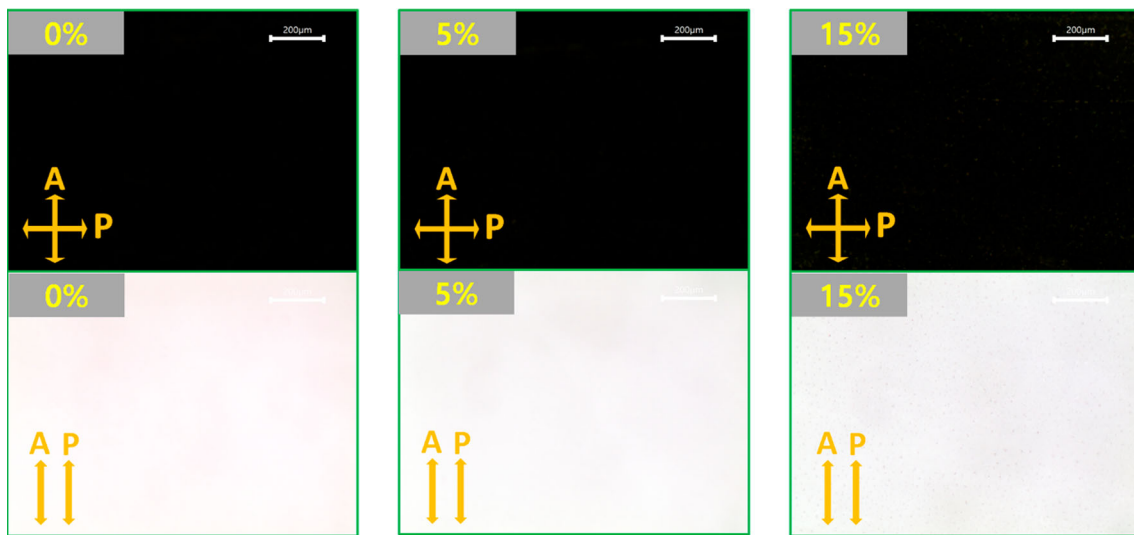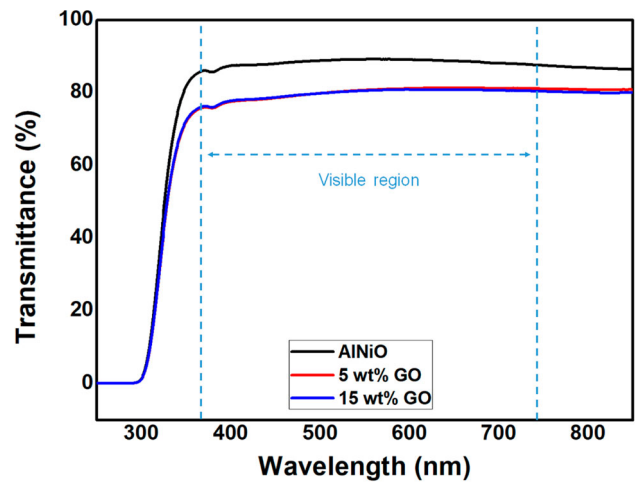

Fig. 2 Liquid crystal alignment state evaluation via polarized optical microscopy for cells assembled using AlNiO films doped with 0, 5, and 15 wt% graphene oxide. The polarizer and analyzer axes are indicated by "P" and "A," respectively
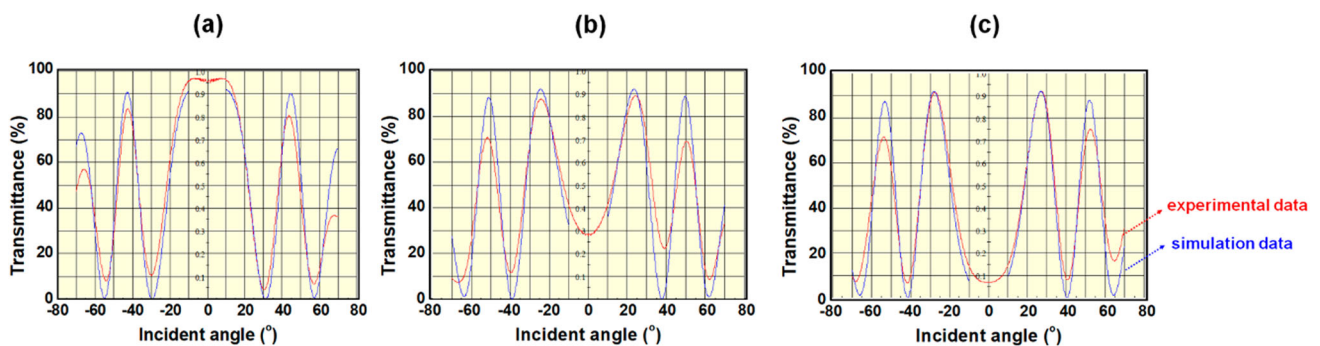
Fig. 3 Liquid crystal pretilt angle analysis using oscillated transmittance graphs for cells assembled using AlNiO films doped with **a** 0, **b** 5, and **c** 15 wt% graphene oxide

based on the hybrid AlNiO films contain uniformly aligned LCs. Therefore, it is demonstrated that the brush-coated GO-doped hybrid AlNiO films can be used as uniform LC alignment layers.

The LC pretilt angles on the hybrid AlNiO alignment layers were analyzed from the oscillated transmittance graphs using the crystal rotation method, as shown in Fig. 3 [18, 19]. The graphs are composed of red and blue lines, which indicate experimental and ideal simulation data, respectively. The simulation data were obtained from the information on the fabricated LC cell gap and injected LC characteristics. The high concordance rate between these two data indicates the stability of the LCs in the cell.
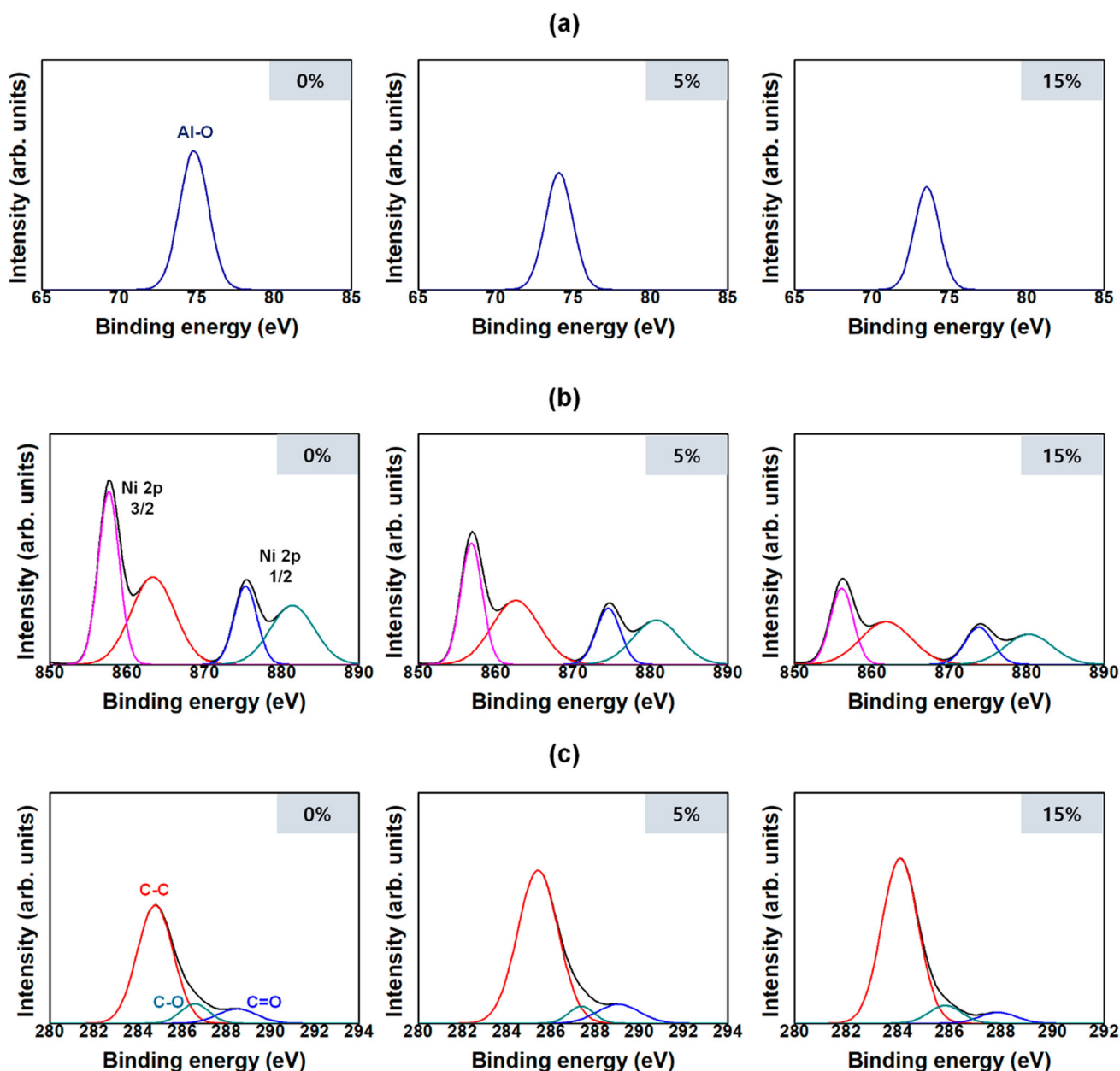
Fig. 4 X-ray photoelectron spectroscopy results of the AlNiO films for the **a** Al 2p, **b** Ni 2p, and **c** C 1 s spectra

The measured samples based on the (a) 0, (b) 5, and (c) 15 wt% GO-doped hybrid AlNiO films revealed very low mismatch rates between the experimental and ideal simulation data. Therefore, the LC pretilt angles were obtained with high reliability. These pretilt angles were 0.27°, 0.16°, and 0.14° for the 0, 5, and 15 wt% GO-doped AlNiO alignment layers, respectively, representing their homogeneous LC alignment states. From the POM and pretilt angle measurements, it is demonstrated that the LCs are uniformly and homogeneously aligned on the hybrid AlNiO alignment layers.

The chemical properties of the brush-coated hybrid AlNiO films containing 0, 5, and 15 wt% GO were analyzed by XPS, as shown in Fig. 4. The Al 2p spectra are presented in Fig. 4a; the peaks are centered in the range of 73.5–74.8 eV, indicating aluminum-oxygen single bonding. These peak intensities decrease as the GO doping concentration increases. The Ni 2p spectra presented in Fig. 4b also show the same tendency. The Ni 2p spectra contain four subpeaks, which represent Ni 2p3/2, Ni 2p1/2, and two satellites. The 3/2 and 1/2 peaks were, respectively, centered in the ranges of 856.0–857.6 eV and 873.8–875.3 eV; their peak intensities decrease as the GO doping concentration increases. The C 1 s spectra shown in Fig. 4c comprise three subpeaks that indicate carbon–carbon single bonds, carbon–oxygen single bonds, and carbon–oxygen double bonds, which are centered in the ranges of 284.1–285.4 eV, 285.8–287.4 eV, and 287.9–289.0 eV, respectively. The peak intensity of the carbon–carbon single bond, which is the main bond
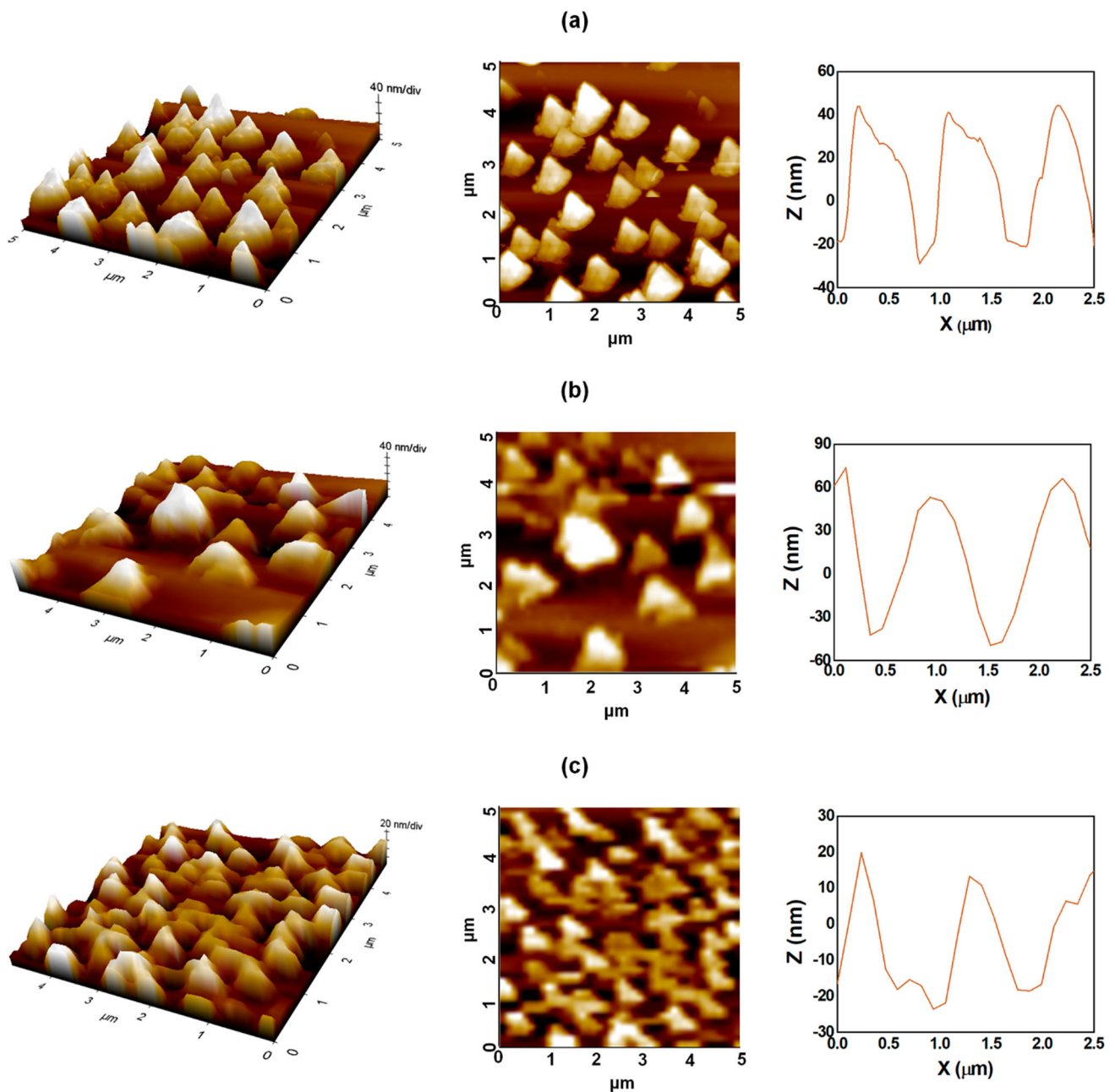
Fig. 5 Surface morphology analyses using atomic force microscopy and corresponding line profiling for AlNiO films doped with **a** 0, **b** 5, and **c** 15 wt% graphene oxide

in GO, increases as the GO doping concentration increases. The XPS results show that the GO-doped hybrid AlNiO films are well constructed, as intended.

The surface structures of the brush-coated hybrid AlNiO films containing 0, 5, and 15 wt% GO were analyzed by AFM and line profiling, as shown in Fig. 5. The pure AlNiO film presented in Fig. 5a reveals directional nano/microgroove morphology on its surface; this structure is derived from the shear stress caused by the brush-hair movement [20, 21]. The directional brush coating results in anisotropic distribution of the AlNiO sol state, and the subsequent thermal curing process converts the sol to gel state, resulting in an anisotropic morphology on the film surface. When the GO doping concentration is 5% (Fig. 5b), the oriented structures are still observed on the surface, although the valley structures of the AlNiO particles are partially collapsed owing to the influence of the polymer chains. When the GO doping concentration is 15% (Fig. 5c), small directional nano/microgroove morphology is observed on the film surface. This reveals that the polymer chains also form directional structures that are induced by the directional fluid flow of the deposited bulk solution [22]. Therefore, it is demonstrated that the anisotropic nano/microgroove structure of the hybrid AlNiO film can be obtained via brush coating. The average roughness values (Ra) were obtained to 24.7, 25.8, and 13.0 for

Fig. 6 Response time analyses of the twisted-nematic liquid crystal (LC) cells based on **a** pure and **b** GO-doped AlNiO films. **c** Threshold voltage evaluation of the LC cells fabricated using AlNiO films doped with 0 and 15 wt% graphene oxide. **d** Polar anchoring energy analysis of the LC cells assembled using AlNiO films doped with 0, 5, and 15 wt% graphene oxide
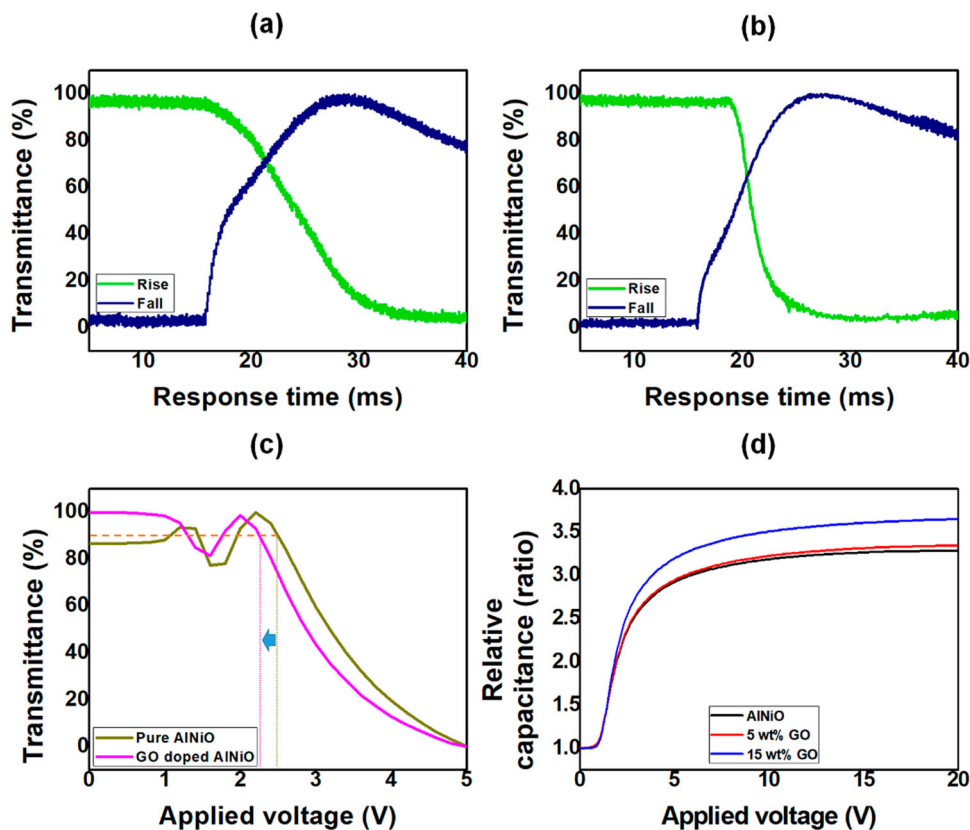
the 0, 5, and 15 wt% GO-doped AlNiO film, respectively. There was no significant difference between 0 and 5%, but there was a big change at 15% doping. Through this, it is confirmed that when the GO doping becomes 15%, the film surface shows a more stable state. The uniform and homogenous LC alignment on the hybrid AlNiO film confirmed via POM and pretilt angle analysis (Figs. 2 and 3) can be attributed to the film surface structure. The LCs have a tendency to minimize elastic distortion, and the geometric constraints of the nano/microgroove structure induce unidirectionally uniform LC alignment on such a surface [23–26].

The EO property is one of the important factors for LC device applications. TN-LC cells fabricated with the 0 (Fig. 6a) and 15 wt% GO-doped (Fig. 6b) AlNiO alignment layers were used to evaluate the fast switching operation ability. The total response time of the LC device can be defined as the sum of the rise and fall times. The rise time is the LC transition time from lying to standing state upon voltage application. The fall time is the LC transition time for the opposite condition. The total response time decreased from 21.4 to 11.8 ms as the GO doping of the AlNiO alignment layer increased. Considering that the conventionally used rubbed PI layer has a response time of 13.4 ms, this result indicates the potential of the GO-doped AlNiO alignment layer [27]. The transmittance–voltage curves of the TN-LC cells based on the 0 and 15 wt% GO-doped AlNiO alignment layers are presented in Fig. 6c. The threshold voltages that corresponds to 90% transmittance were obtained as 2.5 V and 2.3 V for the 0 and 15 wt% GO-doped AlNiO alignment layers, respectively. The LC polar anchoring energy indicates the LC alignment stability on the alignment layer. The energies on the GO-doped hybrid AlNiO alignment layers are shown in Fig. 6d, and these values were obtained as 1.10×10^{-4}, 1.25×10^{-4}, and 5.62×10^{-4} J m^{-2} for the 0, 5, and 15 wt% GO-doped hybrid AlNiO alignment layers, respectively. These results show that GO doping of the AlNiO film enhances the EO and electrical properties for LC device applications.

4 Conclusions

AlNiO hybrid films doped with GO were produced by the brush-coating method, and the doping concentrations were adjusted to 0, 5, and 15 wt%. XPS analysis confirmed the formation of the hybrid film, which had fine optical transmittance for LC device applications. AFM and corresponding line profiling revealed the directional nano/microgroove structure of the film surface, which was induced by the shear stress originating from the brush-coating process; this anisotropic structure induced uniform and homogeneous LC alignment on the surface, which was confirmed by POM and pretilt angle analysis. TN-LC cells fabricated from the hybrid films showed stable and fast switching performances. GO doping of the AlNiO alignment layer was also shown to enhance the LC polar anchoring energy. Therefore, GO-doped AlNiO hybrid films can be used as viable alternatives for next-generation LC alignment layer applications.

Authors' contribution JYO contributed to conceptualization, formal analysis, and writing the original draft. EMK contributed to investigation and validation. GSH and DHK contributed to investigation and visualization. DBY contributed to validation and visualization. BKC contributed to resources and validation.. DWL contributed to formal analysis and supervision. D-SS contributed to funding acquisition and project administration.

Data Availability Statement The raw/processed data required to reproduce these findings are available from the corresponding authors upon reasonable request. The manuscript has associated data in a data repository.

Declarations

Conflict of interest The authors declare that they have no known competing financial interests or personal relationships that could have influenced the work reported in this paper.

References

1. X. Li, W.C.H. Choy, L. Huo, F. Xie, W.E.I. Sha, B. Ding, X. Guo, Y. Li, J. Hou, J. You, Y. Yang, Dual plasmonic nanostructures for high performance inverted organic solar cells. Adv. Mater. **24**, 3046 (2012). https://doi.org/10.1002/adma.201200120
2. S.D. Ponja, B.A.D. Williamson, S. Sathasivam, D.O. Scanlon, I.P. Parkin, C.J. Carmalt, Enhanced electrical properties of antimony doped tin oxide thin films deposited via aerosol assisted chemical vapour deposition. J. Mater. Chem. C. **6**, 7257 (2018). https://doi.org/10.1039/c8tc01929k
3. Y.S. Oh, K.H. Lee, H. Kim, D.Y. Jeon, S.H. Ko, C.P. Grigoropoulos, H.J. Sung, Direct micro/nano patterning of multiple colored quantum dots by large area and multilayer imprinting. J. Phys. Chem. C **116**, 11728 (2012). https://doi.org/10.1021/jp301397t
4. U.N. Tohgha, E.P. Crenshaw, M.E. McConney, K.M. Lee, N.P. Godman, Tuning of optical properties and phase behavior of nanomaterial-stabilized blue phase liquid crystals. J. Colloid Interface Sci. **639**, 401 (2023). https://doi.org/10.1016/j.jcis.2023.02.076
5. H. Zhou, S. Zheng, X. Guo, Y. Gao, H. Li, H. Pang, Ordered porous and uniform electric-field-strength micro-supercapacitors by 3D printing based on liquid-crystal V_2O_5 nanowires compositing carbon nanomaterials. J. Colloid Interface Sci. **628**, 24 (2022). https://doi.org/10.1016/j.jcis.2022.08.043
6. N.K .Chaudhari, A. Oh, Y.J. Sa, H. Jin, H. Baik, S.G. Kim, S.J. Lee, S.H. Joo, K. Lee, Morphology controlled synthesis of 2-d Ni–Ni_3S_2 and Ni_3S_2 nanostructures on Ni foam towards oxygen evolution reaction. Nano Converg. **4**, 7 (2017). https://doi.org/10.1186/s40580-017-0101-6
7. K. Yu, Z. Zhang, Y. Zhao, J. Wang, W. Huang, Z. Mo, Y. Chen, K. Wang, X. Liu, Z. Cao, J. Shao, Optical properties and nanosecond laser damage characterization of liquid crystal polarization gratings. Opt. Mater. **147**, 114755 (2024). https://doi.org/10.1016/j.optmat.2023.114755
8. C.P. Ganea, D. Manaila-Maximean. V. Cîrcu, Dielectric investigations on carbon nanotubes doped polymer dispersed liquid crystal films. Eur. Phys. J. Plus **135**, 797 (2020). https://doi.org/10.1140/epjp/s13360-020-00795-w
9. M. Surekha, D.M. Potukuchi, Exploration of Goldstone mode and field-induced SmA-SmC*-SmC Lifshitz point in chiral liquid crystal dimers for multiple polarization switching. Eur. Phys. J. Plus **137**, 656 (2022). https://doi.org/10.1140/epjp/s13360-022-02728-1
10. M. Honma, T. Otsuka, R. Ito, S. Pau, T. Nose, Alignment of semiconducting liquid crystalline polymers induced by hot stylus rubbing. Jpn. J. Appl. Phys. **63**, 3 (2024). https://doi.org/10.35848/1347-4065/ad272b
11. K.V. Rao, A. Smakula, Dielectric properties of cobalt oxide, nickel oxide, and their mixed crystals. J. Appl. Phys. **36**, 2031 (1965). https://doi.org/10.1063/1.1714397
12. C.W .Chen, H.W. Tsai, Y.C. Wang, Y.C. Shih, T.Y. Su, C.H. Yang, W.S. Lin, C.H. Shen, J.M. Shieh, Y.L. Chueh, Rear-passivated ultrathin Cu(In, Ga)Se_2 films by Al_2O_3 nanostructures using glancing angle deposition toward photovoltaic devices with enhanced efficiency. Adv. Funct. Mater. **29**, 1 (2019). https://doi.org/10.1002/adfm.201905040
13. H. Faber, B. Butz, C. Dieker, E. Spiecker, M. Halik, Fully patterned low-voltage transparent metal oxide transistors deposited solely by chemical spray pyrolysis. Adv. Funct. Mater. **23**, 2828 (2013). https://doi.org/10.1002/adfm.201202334
14. Y.H. Shim, K.E. Lee, T.J. Shin, S.O. Kim, S.Y. Kim, Tailored colloidal stability and rheological properties of graphene oxide liquid crystals with polymer-induced depletion attractions. ACS Nano **12**, 11399 (2018). https://doi.org/10.1021/acsnano.8b06320
15. S.-H. Hong, T.-Z. Shen, J.-K. Song, Electro-optical characteristics of aqueous graphene oxide dispersion depending on ion concentration. J. Phys. Chem. C **118**, 26304 (2014). https://doi.org/10.1021/jp504892s
16. T.-Z. Shen, S.-H. Hong, J.-K. Song, Electro-optical switching of graphene oxide liquid crystals with an extremely large Kerr coefficient. Nat. Mater. **13**, 394 (2014). https://doi.org/10.1038/nmat3888
17. D.W. Lee, J.H. Lee, E.M. Kim, G.S. Heo, D.H. Kim, J.Y. Oh, Y. Liu, D.-S. Seo, Surface modification of a poly(ethylene-co-vinyl acetate) layer by ion beam irradiation for the uniform alignment of liquid crystals. J. Mol. Liq. **339**, 116700 (2021). https://doi.org/10.1016/j.molliq.2021.116700
18. K.-H. Chen, W.-Y. Chang, J.-H. Chen, Measurement of the pretilt angle and the cell gap of nematic liquid crystal cells by heterodyne interferometry. Opt. Express **17**, 14143 (2009). https://doi.org/10.1364/OE.17.014143
19. J.-H. Kim, M. Yoneya, J. Yamamoto, H. Yokoyama, Nano-rubbing of a liquid crystal alignment layer by an atomic force microscope: a detailed characterization. Nanotechnology **13**, 133 (2002). https://doi.org/10.1088/0957-4484/13/2/301
20. C.C. Mell, S.R. Finn, Forces exerted during the brushing of a paint. Rheol. Acta **4**, 260 (1965). https://doi.org/10.1007/BF01973663
21. S.-S. Kim, S.-I. Na, J. Jo, G. Tae, D.-Y. Kim, Efficient polymer solar cells fabricated by simple brush painting. Adv. Mater. **19**, 4410 (2007). https://doi.org/10.1002/adma.200702040
22. Y.J. Cha, D.K. Yoon, Control of periodic zigzag structures of DNA by a simple shearing method. Adv. Mater. **29**, 1604247 (2017). https://doi.org/10.1002/adma.201604247
23. D.W. Berreman, Solid surface shape and the alignment of an adjacent nematic liquid crystal. Phys. Rev. Lett. **28**, 1683 (1972). https://doi.org/10.1103/PhysRevLett.28.1683
24. J.-I. Fukuda, M. Yoneya, H. Yokoyama, Surface-groove-induced azimuthal anchoring of a nematic liquid crystal: Berreman's model reexamined. Phys. Rev. Lett. **98**, 187803 (2007). https://doi.org/10.1103/PhysRevLett.98.187803
25. B. Chae, S.B. Kim, S.W. Lee, S.I. Kim, W. Choi, B. Lee, M. Ree, K.H. Lee, J.C. Jung, Surface morphology, molecular reorientation, and liquid crystal alignment properties of rubbed nanofilms of a well-defined brush polyimide with a fully rodlike backbone. Macromolecules **35**, 10119 (2002). https://doi.org/10.1021/ma020639i

26. H. Kikuchi, J.A. Logan, D.Y. Yoon, Study of local stress, morphology, and liquid-crystal alignment on buffed polyimide surfaces J. Appl. Phys. **79**, 6811 (1996). https://doi.org/10.1063/1.361502

27. Y. Liu, J.H. Lee, D.-S. Seo, Ion beam fabrication of aluminum-doped zinc oxide layer for high-performance liquid crystals alignment. Opt. Express **24**, 17424 (2016). https://doi.org/10.1364/OE.24.017424